

A Statistical Study of Solar Filament Eruptions That Forms High-Speed Coronal Mass Ejections

PENG ZOU,¹ CHAOWEI JIANG*,¹ FENGSI WEI,¹ PINGBIN ZUO,¹ AND YI WANG¹¹*Institute of Space Science and Applied Technology, Harbin Institute of Technology, Shenzhen 518055, China*

ABSTRACT

Coronal mass ejections (CMEs) play a decisive role in driving space weather, especially, the fast ones (e.g., with speeds above 800 km s^{-1}). Understanding the trigger mechanisms of fast CMEs can help us gaining important information in forecasting them. The filament eruptions accompanied with CMEs provide a good tracer in studying the early evolution of CMEs. Here we surveyed 66 filament-accompanied fast CMEs to analyse the correlation between the trigger mechanisms, namely either magnetic reconnection or ideal MHD process, associated flares, and CME speeds. Based on the data gathering from SDO, GONG and STEREO, we find that: (1) Active region (AR) filament and intermediate filaments (IFs) eruptions show a higher probability for producing fast CMEs than quiet Sun (QS) filaments, while the probability of polar crown (PC) filament eruptions is zero in our statistic; (2) AR filament eruptions that produce fast CMEs are more likely triggered by magnetic reconnection, while QS and IFs are more likely triggered by ideal MHD process; (3) For AR filaments and IFs, it seems that the specific trigger mechanism does not have a significant influence on the resulted CME speeds, while for the QS filaments, the ideal MHD mechanism can more likely generate a faster CME; (4) Comparing with previous statistic study, the onset heights of filament eruptions and the decay indexes of the overlying field show some differences: for AR filaments and IFs, the decay indexes are larger and much closer to the theoretical threshold, while for QS filaments, the onset heights are higher than those obtained in previous results.

Keywords: Sun: filaments, prominences; Sun: coronal mass ejections (CMEs); Sun: flares

1. INTRODUCTION

Coronal mass ejections (CMEs), which are the most violent, eruptive phenomenon on the Sun, can throw out over $10^{12} - 10^{13} \text{ kg}$ of magnetized plasma into the interplanetary (Jackson 1985; Gopalswamy & Kundu 1992; Hudson et al. 1996). The very high-speed CMEs, if directed to the Earth, can cause strong geomagnetic storms and severely threaten space weather (Tsurutani et al. 1988; Gonzalez et al. 1999; Huttunen et al. 2002, 2005; Liu et al. 2014). To avoid such disaster caused by them, prediction of CMEs, especially the fast ones, is an important topic in space weather research (Singer et al. 2001; Schwenn et al. 2005). Particularly, it is crucial to investigate the pre-eruptive conditions and the trigger mechanisms of CMEs for a reliable prediction.

CMEs originate from the solar corona, and are often accompanied with other activities, such as flares and filament eruptions (Harrison 1995; Yashiro et al. 2005; Wang & Zhang 2007; Gopalswamy et al. 2003; Jing et al. 2004). Now it is commonly believed that these eruptive phenomena are all

driven by the evolution of solar coronal magnetic field, which suddenly released its free energy through eruptions. In order to understand how the eruptions are triggered, many theoretical models have been proposed (Sakurai 1976; van Ballegoijen & Martens 1989; Antiochos et al. 1999; Chen & Shibata 2000; Moore et al. 2001; Toörök & Kliem 2005; Kliem & Toörök 2006; Aulanier et al. 2010), which can roughly be divided into two categories: one is based on magnetic reconnection, and the other is via ideal MHD process (Sakurai 1976; Toörök & Kliem 2005; Kliem & Toörök 2006; Aulanier et al. 2010). The reconnection mechanisms, including mainly the tether-cutting model (Moore et al. 2001) and break-out model (Antiochos et al. 1999), consider that magnetic reconnection plays a fundamental role in producing the eruption of magnetic structures. The tether-cutting model suggests that reconnection within sheared magnetic arcades can break the balance between the outward magnetic pressure force and the inward magnetic tension of the overlying field (Moore et al. 2001). It describes the situation that two magnetic arcades get close to each other via photospheric shearing and converging flows. When the sheared arcades are close enough, magnetic reconnection will take place to build up a magnetic flux rope (MFR) or even trigger an eruption. This model has

*Corresponding authors: chaowei@hit.edu.cn

been well studied during last decades, as numerous observations have shown shearing and converging flows a few hours or minutes before triggering of flares and CMEs (Wang et al. 2005; Liu et al. 2013; Shimizu et al. 2014). And accompanied magnetic cancellations and increasing radiations indicate that magnetic reconnection takes place and finally triggers the eruptions (Leka et al. 1996; Sterling et al. 2010). Note that the reconnection is within the core structure. On the other hand, the break-out model proposes that reconnection above the sheared arcades can do the same work by weakening the overlying field (Antiochos et al. 1999). Such process studied by simulations is also consistent with observations (Lynch et al. 2004). Based on coronal magnetic field extrapolations, it is demonstrated that this model can explain observations of CMEs (Zhou et al. 2017). Unlike the tether-cutting model, there are fewer precursors that can be observed for this model (Sterling & Moore 2001a). Besides, magnetic flux emergence and its associated magnetic reconnection are also proposed as being the trigger of eruption. For example, Chen & Shibata (2000) proposed a model in which the emergence flux inside or outside the core structure (a MFR) can trigger its eruption, i.e., an inside emerging flux can cause converging flow underneath the MFR and then trigger reconnection, while an outside emerging flux can weaken the overlying field via reconnection. Note that all these mentioned models are based magnetic reconnection. The ideal MHD models believe that the eruptions can be triggered and accelerated by the ideal magnetohydrodynamics (MHD) instabilities, such as kink instability and torus instability associated with twisted magnetic flux rope (MFR) (Sakurai 1976; Torök & Kliem 2005; Kliem & Torök 2006; Aulanier et al. 2010). In such models, the magnetic reconnection is triggered as a result of the eruptions. The simulation of Aulanier et al. (2010) suggests that the ideal MHD instability plays a more important role in forming CMEs. And in the investigation of the strongest flare in 24 solar cycle by Yang et al. (2017), they think the associated CME was firstly caused by the kink instability of the filament embedded in.

Although there are numerous studies on the early evolution of CMEs, only a few of them focus on quiescent filament eruption. Basing on previous studies we can know that they are not so different from the AR eruptions. They can have similar evolve processes, reach a high enough speed or associated with a double-ribbon flare. However, some studies found that the accompanied flares have some delay with the eruption onset (Sterling & Moore 2001b). It seems the reconnection is the result of the eruption, just like the description of those eruptions triggered by idea MHD instabilities. And Zhou et al. (2006) and Su et al. (2015) are confirmed these instabilities, such as kink instability and torus instability, can trigger eruptions of quiescent filaments.

Filaments, or prominences when seen above the solar limb, are fascinating objects embedded in the solar corona. They are roughly 100 times denser than the surrounding corona but 100 times colder. In order to sustain such heavy materials, special magnetic structures are needed to provide upward magnetic tension force, for example, the magnetic dips within MFRs (Kippenhahn & Schluter 1957; Kuperus & Raadu 1974). Since filament eruptions can be well observed by multi-wavelength, such as $H\alpha$, 304Å, 193Å and 211Å, once the MFR holding a filament becomes unstable and erupts, the erupting filament as observed provides a tracer of the dynamic evolution of the underlying magnetic structure. Furthermore, many statistical studies have shown that the occurrence of filament eruptions are strongly related with that of CMEs (Gopalswamy et al. 2003; Jing et al. 2004; Chen 2011), and the erupting filament materials are recognized in most cases as the bright core of typical CMEs. Thus observation of the filament eruptions provides the key in studying the early kinetic evolution of CMEs.

Regarding to the triggering mechanisms by either reconnection or ideal MHD, the filament eruptions should behave rather differently in observations. For reconnection-triggered ones, their eruptions should be preceded by a strong enhancement of X-ray (as well as EUV) intensity close to or on the filament spine. For ideal MHD process, the intensity enhancement or X-ray flux increasing will occur a bit after its eruption. Thus for typical events, the triggers can be easily distinguished. In their evolutions, the idea MHD process can always provide a clear trajectory of erupting filament (Cheng et al. 2013), which can be used to study its acceleration. While for reconnection process, more precursors can be observed in photospheric magnetic field, such as emerging parasitic poles or conversion flows (Feynman & Martin 1995; Jing et al. 2004). These precursors are helpful in predicting its trigger.

The Heliophysics Event Knowledgebase (HEK, Hurlburt et al. 2012), which is a catalog of the records of solar activities, including the filament eruption records from 2011 to now. Using the records, some statistical studies discussed the relationship between eruptive filaments and formed CMEs. For example, McCauley et al. (2015) surveyed some properties of more than 900 filament eruptions recorded by HEK. Among them, more than 100 limb events are analyzed for studying their onset radial height and decay index. It is found that the onset heights show a significant difference in different filament types. On the other hand, the differences for decay indexes are not so significant. The decay indexes have an average value of 1.1 for all the filament, with the quiescent type slightly higher and the active region type slightly lower. For the eruptive filaments, some of them can form the CMEs and some of them failed. Jing et al. (2018) studied 38 eruption events that are associated with flares stronger

than M5 class. They found that all the core magnetic structures of confined events are underneath the height with decay index equal 0.8. But the eruptive ones do not show a well-defined threshold, e.g., they can occur with decay index even smaller than 0.8. Although, it is concluded that reconnection solely seems not able to strong enough for ejecting a CME in the study of [Aulanier et al. \(2010\)](#), the statistical result suggests that reconnection can break out the constrain of strong overlying magnetic field, i.e., the eruptive events with decay index smaller than 0.8 are triggered by reconnection. Thus a survey of the triggering mechanisms of filament eruptions is required to provide new insights for this topic.

In this paper, we carried out a statistical study to identify the triggering mechanisms for filament eruptions with focus on those resulting in high-speed CMEs. We will statistically analyse the relationships among CME velocities, filament types, trigger mechanism and some magnetic properties. The first part (Section 2) will introduce the data, standards in dividing the events and methods in calculating the magnetic properties. Second part (Section 3) will gather the results of the statistical properties. The last part (Section 4) will summarize our findings.

2. DATA AND METHOD

The filament eruption samples are obtained from HEK. Here we first selected the significantly high-speed CME events (velocity $> 800 \text{ km s}^{-1}$ which is larger than the speed of fast solar wind) in time span from June 1 2011 to June 1 2017 and identified their origin sites. Then, only the CMEs which are accompanied with filament eruptions are confirmed as the samples. A total number of 87 events are selected from over 400 CMEs. Among these 87 events, some of them took place behind the solar disk and a few of them are hardly to be traced for their trajectory. As such, we discarded these events since they will cause errors in identifying their flare class and onset time. After this filtering, we finally obtained 66 events for statistic study. All of their eruption evolutions can be observed by Atmospheric Imaging Assembly (AIA, [Lemen et al. 2012](#)) onboard the Solar Dynamics Observatory (SDO, [Pesnell et al. 2012](#)). Furthermore, in order to gain the accurate position information of the pre-eruptive filaments, 195 Å images taken by Solar Terrestrial Relations Observatory (STEREO, [Howard 2008](#)) are also used. All the events are listed in Table 1.

2.1. Filament types

Filaments (or prominences) distribute in the whole solar disc, including the polar regions as well as the equator ([Engvold 2015](#)). They are often grouped in four types according to their locations. Active region (AR) filaments form in ARs. Quiet Sun (QS) filaments are located in quiet sun regions far away from ARs. There are also intermediate filaments (IF)

that have one leg rooted in AR and the other one rooted in quiet sun region, or lie between neighboring ARs. Filaments found at the polar regions, e.g., at latitudes larger than 50° , are called polar crown (PC) filaments. Different types of filaments can have different physical properties, e.g., magnetic configurations and strength. Thus dividing the samples by filament types can help us clarifying the important factors that affect their eruption. A typical filament for each type is shown in Figure 1, and the statistical numbers are given in Figure 2. Note that there is no PC filament in our statistic samples, probably due to the fact that the weak magnetic field strength in high latitude is unable to produce fast CMEs.

2.2. Time-distance evolutions

Time-distance maps provide the kinetic information of a drifting object with time. It is widely used in tracing eruptive events, such as jets, flares and filament eruptions. In a majority of the cases, a straight line pointing along the eruption direction can fully cover the evolution trajectory of an erupting filament. However, for a few events, the trajectories are not along a straight line. In such cases, we select 4 or 5 frames during the eruption and mark the front of eruption by hand. Then a conic is used to fit all the mark points. In order to cover the whole trajectory of eruptions, we extended this conic from the footpoint to the front until it moves out of the view. Figure 3 shows one of the events analyzed for time-distance evolution. The upper panels show the selected frames, where the marks are shown by the green diamonds. The yellow dashed line shows the location for picking up the slice. The bottom panel displays the time-distance map along the yellow dashed line.

Evolution of an erupting filament often demonstrates two distinct phases: a slow-rise phase and a fast-rise phase. The slow-rise phase can be recognized as the upward motion with a constant and small velocity ([Sterling & Moore 2005](#)), while the fast-rise phase can be fitted with an exponential function ([Goff et al. 2005](#); [Williams 2005](#)). In order to fit these two phases with a single curve, we use the function proposed by [Cheng et al. \(2013\)](#):

$$h(t) = c_0 e^{(t-t_0)/\tau} + c_1 (t-t_0) + c_2, \quad (1)$$

where $h(t)$ is the height of filament, t is the time and c_0 , c_1 , c_2 , t_0 and τ are free parameters. With this function, we can calculate conveniently the eruption onset time ([McCauley et al. 2015](#)), which is defined by

$$t_{\text{onset}} = \tau \ln(c_1 \tau / c_0) + t_0. \quad (2)$$

It means the instantaneous velocity at the onset time is twice of the initial value, i.e., the constant speed in the slow-rise phase. In the bottom panel of Figure 3, we denote the onset time using a cyan dashed line. This function can well fit some

Table 1. The list of all events of filament eruptions.

Date	Type	AR ^a No.	FC ^a	FOT ^a	FPT ^a	CME V (km/s)	Mechanism	OT ^a	OH ^a (Mm)	DI ^a
2011/06/07	AR	AR11226	M2.5	06:16	06:34	1255	R ^a	06:16:46	18.1	0.77
2011/07/06	QS ^a	/	/	/	/	835	NR ^a	09:56:13	182.0	1.25
2011/08/04	AR	AR11261	M9.3	03:41	03:57	1315	R	03:46:58	39.3	1.86
2011/08/11	AR	AR11263	C6.2	09:34	10:23	1160	R	09:55:33	22.6	1.34
2011/09/13	IF ^a	AR11288	C2.7	12:03	13:02	1024	NR	12:01:18	49.8	1.26
2011/10/01	AR	AR11309	B8.5	20:30	20:32	1238	NR	20:26:42	72.5	2.47
2011/11/09	IF	AR11342	M1.1	13:04	13:35	907	R	13:06:52	82.9	1.30
2012/01/01	QS	/	/	/	/	801	NR	00:31:50	70.8	0.74
2012/01/19	AR	AR11402	M3.2	13:44	16:03	1120	R	14:30:33	/	/
2012/01/23	IF	AR11402	M8.7	03:38	03:58	2175	R ^b	03:37:56	71.7	1.46
2012/01/27	AR	AR11402	X1.7	17:37	18:36	2508	NR ^c	17:44:13	66.7	1.56
2012/02/19	QS	/	/	/	/	846	NR	16:33:59	42.9	1.68
2012/03/16	QS	/	/	/	/	862	NR	19:02:40	344.1	1.69
2012/03/27	AR	AR11444	C5.3	02:50	03:08	1148	R	02:50:44	41.7	1.91
2012/04/05	AR	AR11450	C1.5	20:49	21:10	828	NR	20:48:47	87.2	1.92
2012/04/09	QS	/	/	/	/	921	NR	14:28:27	159.6	1.05
2012/04/16	AR	AR11461	M1.7	17:24	17:40	1348	R	17:24:32	17.0	2.07
2012/05/11	QS	/	C3.2	23:02	23:44	805	R	23:17:13	/	/
2012/06/23	AR	AR11506	C2.7	07:02	07:46	1263	R	06:58:32	115.8	0.78
2012/07/02	QS	/	/	/	/	988	NR	06:12:43	129.3	1.69
2012/07/12	QS	/	/	/	/	843	NR	14:50:38	39.0	0.84
2012/08/17	IF	AR11542	B6.0	21:51	22:28	986	R	21:52:43	/	/
2012/08/31	IF	AR11562	C8.5	19:33	20:43	1442	NR	19:14:06	80.2	2.20
2012/09/27	IF	AR11577	C3.7	23:28	23:57	947	NR	23:19:31	56.3	0.76
2012/11/27	QS	/	C5.9	02:10	02:15	844	NR	01:16:34	75.3	0.85
2012/12/04	IF	AR11628	C1.8	00:05	00:28	963	NR	23:49:43	98.9	0.88
2013/01/06	QS	/	/	/	/	860	NR	05:37:35	103.8	0.88
2013/02/06	AR	AR11667	C8.7	00:04	00:20	1867	R	00:09:11	/	/
2013/02/11	AR	AR11667	B5.8	18:56	19:05	1161	NR	18:53:57	19.6	1.90
2013/02/12	QS	/	/	/	/	1050	NR	21:42:07	38.0	2.08
2013/03/12	AR	AR11690	C2.0	10:17	10:39	1024	NR	10:16:23	94.1	2.11
2013/07/18	QS	/	C2.3	19:57	20:14	939	NR	17:52:03	68.1	1.58
2013/08/17	AR	AR11818	M3.3	18:16	18:24	1202	R	18:21:36	19.3	1.31
2013/09/10	QS	/	/	/	/	847	NR	11:59:04	32.5	0.66
2013/09/24	QS	/	/	/	/	919	NR	20:03:25	136.8	0.69
2013/09/29	QS	/	C1.2	21:43	23:30	1179	NR	21:23:55	51.2	0.89
2013/10/28	AR	AR11875	M5.1	04:32	04:41	1201	R	04:38:10	24.2	0.59
2013/10/28	AR	AR11882	M4.4	15:07	15:15	812	R ^d	14:54:31	/	/
2013/12/23	QS	/	/	/	/	1409	NR	07:47:07	91.7	f ^e
2014/01/03	QS	/	/	/	/	1132	NR	03:11:26	46.5	2.41
2014/01/30	AR	AR11967	M6.6	15:52	16:11	1087	NR	15:49:27	44.0	1.50
2014/02/25	AR	AR11990	X4.9	00:39	00:49	2147	R	00:41:57	17.8	0.40
2014/03/04	QS	/	/	/	/	911	NR	20:58:24	20.0	1.53
2014/04/02	AR	AR12027	M6.5	13:18	14:03	1471	NR	13:15:45	61.3	1.70
2014/04/12	AR	AR12035	C5.0	07:04	07:31	1016	R	07:14:21	40.2	1.52
2014/04/18	QS	/	f ^f	/	/	926	R	08:54:19	/	/
2014/06/08	AR	AR12087	C5.2	23:46	23:54	836	R	23:47:51	11.5	0.81
2014/06/13	QS	/	f ^g	/	/	992	NR	18:11:04	119.0	0.90
2014/07/10	QS	/	/	/	/	928	NR	05:57:37	157.0	1.75
2014/12/12	IF	AR12232	C1.2	03:42	04:51	1133	NR	03:22:00	/	/

Table 2. Continued of Table 1.

Date	Type	AR ^a No.	FC ^a	FOT ^a	FPT ^a	CME V (km/s)	Mechanism	OT ^a	OH ^a (Mm)	DI ^a
2014/12/20	QS	/	/	/	/	830	R	00:58:01	26.9	0.26
2015/01/12	AR	AR12261	C3.7	15:18	15:21	1078	NR	15:10:09	53.3	1.05
2015/04/04	QS	/	C3.8	22:16	23:48	825	R	22:20:31	69.9	0.64
2015/06/03	QS	/	<i>f</i> ^b	/	/	818	NR	22:20:31	118.9	1.34
2015/06/18	AR	AR12365	M1.3	00:20	01:27	1714	R	00:20:34	24.6	1.73
2015/07/25	QS	/	/	/	/	889	NR	13:32:30	64.6	1.56
2015/08/07	QS	/	/	/	/	876	NR	19:27:10	167.1	1.02
2015/08/09	IF	AR12393	B8.1	11:03	11:43	810	NR	10:51:06	54.4	1.93
2015/08/23	QS	/	C1.4	04:07	04:22	832	R	04:08:06	/	/
2015/10/07	QS	/	/	/	/	900	NR	07:12:15	174.6	0.95
2016/04/18	QS	/	<i>f</i> ^g	/	/	822	NR	01:38:09	29.9	1.27
2016/05/11	IF	AR12540	<i>f</i> ^h	/	/	967	NR	10:34:41	87.1	1.34
2016/05/24	QS	/	/	/	/	914	NR	04:16:57	75.0	0.96
2017/04/17	IF	AR12651	B7.6	21:23	21:42	1014	R	21:31:30	38.6	0.99
2017/04/20	AR	AR12652	/	/	/	1041	NR	16:15:27	21.7	<i>f</i> ⁱ
2017/04/24	QS	/	/	/	/	1008	NR	01:38:26	69.8	0.68

^a AR: AR filament, IF: Intermediate filament, QS: QS filament, R: reconnection, NR: non-reconnection, FC: flare class, FOT: flare onset time, FPT: flare peak time, OT: onset time, OH: onset height, DI: decay index

^b Before the eruption and main flare, there is a weaker flare underneath the filament. After the flare ribbon propagate through the filament north part, the filament erupted. Therefore, we believe that this filament was triggered by the reconnection.

^c Before the flare triggered, the filament show obvious kink motion, therefore this eruption is considered as a non-reconnection triggered one.

^d At about 14:50, before the onset time of flare and eruption, the south footpoint of filament start flaring and a slow X-ray flux increase is associated. Therefore, we believe this filament eruption is triggered by this reconnection.

^e The surrounding magnetic field is too weak to avoid the error from the noise of magnetic field strength.

^f The eruption do associate a small flare, but we cannot determine whether the soft X-ray flux rising is caused by this flare or the decay phase of the previous flare in other ARs.

^g The GOES flux is covered by other flares

^h There is no GOES record.

ⁱ There is no PFSS data.

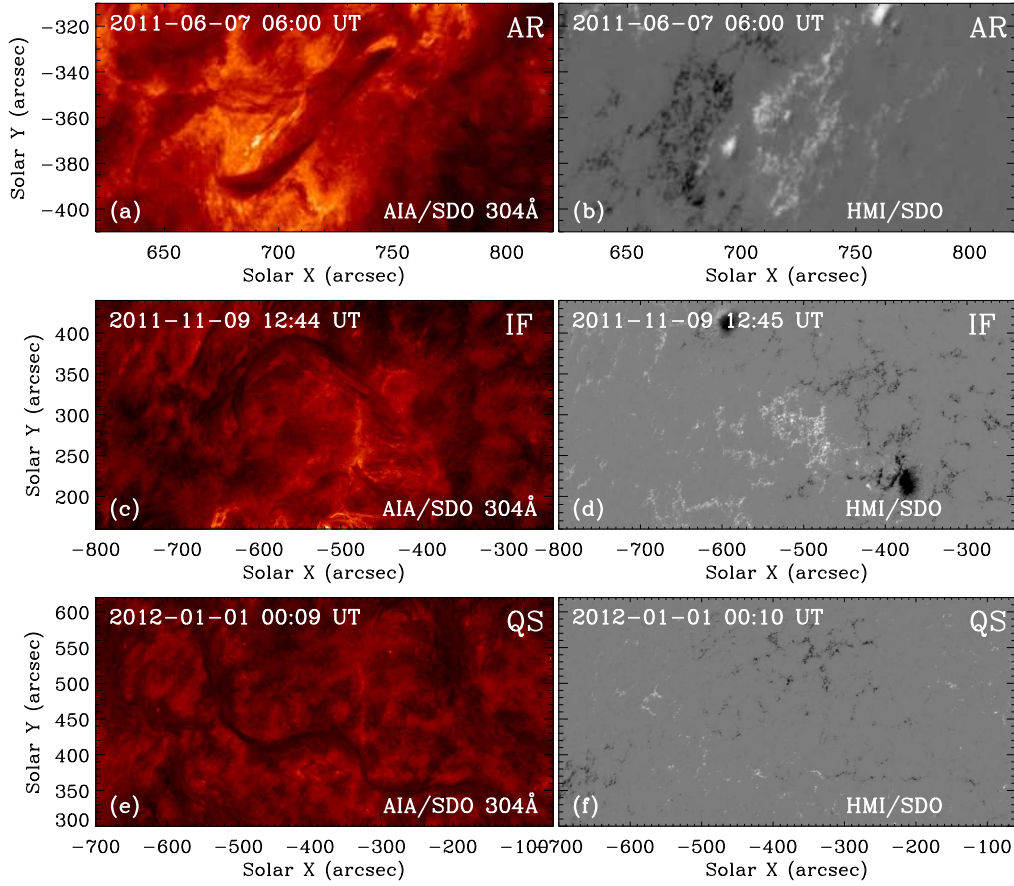


Figure 1. The samples of typical filaments in different types observed in 304Å and 193Å filtergrams.

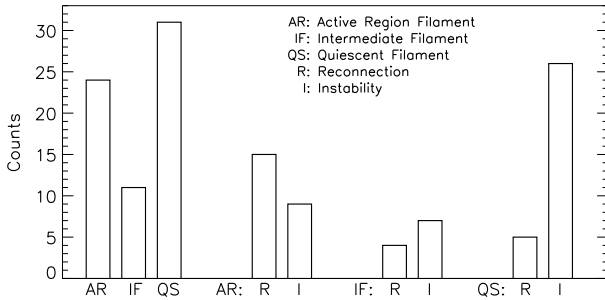


Figure 2. The histogram of filament types and mechanisms of different types.

of the eruption evolves, more well-fit results are shown in Figure 4

However, it should be noted that not all filament eruptions demonstrate such well-defined two-phase pattern. In our samples, about 33% cannot be fitted with the two-phase function. For instance, some typical reconnection-triggered eruptions do not have a slow-rise phase, since they are ac-

celerated rather abruptly. As an example shown in Figure 5, the initiation of such reconnection-triggered events are accompanied with strong EUV intensity enhancement, and in these cases, the trajectory of erupting filaments is similar, i.e., starting with an almost static or extremely slow rise phase, then followed by a rapid acceleration immediately after the intensity enhancement, and finally reaching a constant velocity. We have attempted to define their onset time using the aforementioned method but failed, because as shown in Figure 5 some of their acceleration phases are covered by the strong radiations. Besides, there are also some fast accelerated eruptions which cannot be fitted well by an exponential curve. For example, see such an event shown in Figure 6. This event includes 4 phases during its eruption. The first phase was a very slow rise phase (nearly undetectable), then it was most probably triggered by a reconnection (see the intensity enhancements underneath the filament). After a short acceleration, it ejected with nearly constant speed. Several minutes later, it seems to be accelerated again, but meanwhile was split into three parts. Then all these parts show

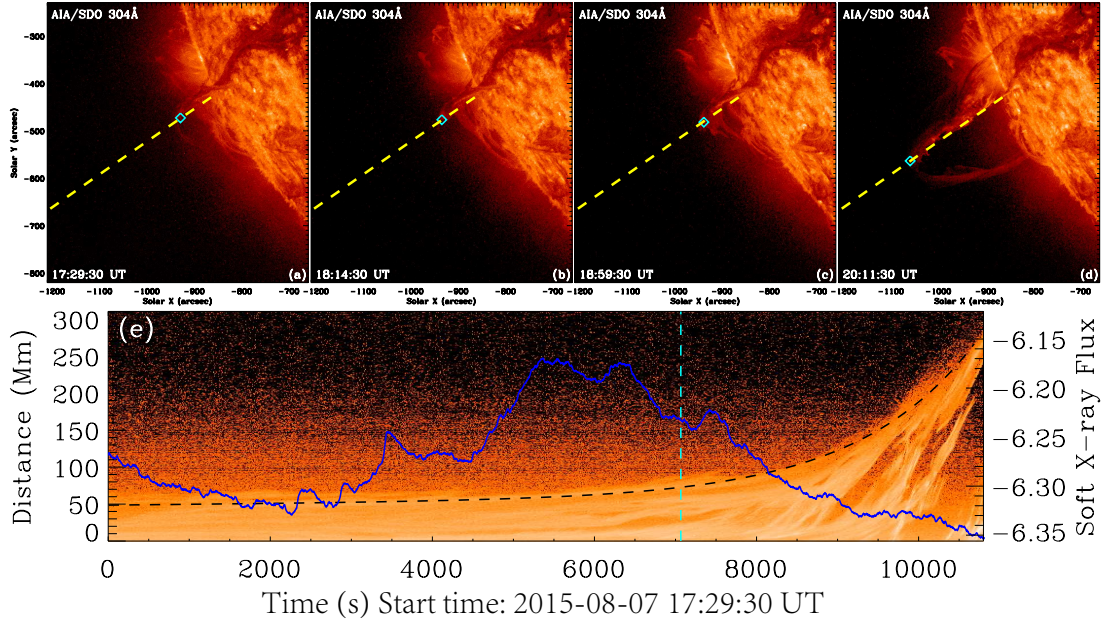


Figure 3. The example for evaluating the time-distance maps. The top panels show the marks in cyan diamond and the slice in yellow dashed line. Panel e show the time-distance map of the sample. The blue line is GOES soft X-ray flux, the black dashed line is time-distance fitting curve and the cyan dashed line shows the onset time.

uniform velocities. The cases with such complex trajectories can hardly be defined with an onset time using the aforementioned method. Thus, for all these cases, we define the eruption onset time as beginning of the intensity enhancement, i.e., the same onset time of flare reconnection. Since in these cases, the filaments are almost static before eruption and the accelerations are so rapid, there is no significant uncertainty brought in calculating its onset height.

2.3. Onset height and decay index

It has been suggested that ideal MHD instabilities play an important role in triggering filament eruptions. In particular, the torus instability has been proposed to be the most important one for producing CMEs. For an ideal MFR configuration, the torus instability is determined by the decay index, which describes the decreasing speed (with height) of background magnetic field overlying the MFR. Specifically, the MFR system becomes unstable when the apex of the rope axis reaches a height where the decay index exceeds a threshold value (Toörök & Kliem 2005; Kliem & Toörök 2006). Thus it is meaningful to calculate the onset height of eruption prominence, and derive the decay index at this height.

Joint observations of STEREO and SDO are used to obtain the onset height. Figures 8 and 9 show two examples of evaluating the onset height. First, we use a diamond to mark the body of prominence and then trace the latitude to mark the same position of filament in STEREO. This new mark can tell us the longitude of the filament, and associated with the relative position of STEREO and SDO, we can get the longitude and latitude of the prominence observed in SDO. Thus

the position and height of prominence can be derived. However, this method can be used only for those prominences observed in both SDO and STEREO, while some events do not have STEREO observations with an appropriate angle. For prominences (above the limb) of these events, we calculate their radial height projected to the plane-to-sky. For radial eruptive filaments (onboard the disc), we can calculate the distance between filament spine and footpoints and project it back to 3D space. Even so, there are still 8 events (3 AR filaments, 2 IF filaments and 3 QS filaments) for which the onset height cannot be determined.

After evaluating the onset height of filaments, we can calculate the decay index n , which is defined as $n = -\partial \ln B / \partial \ln h$, at their onset height h . The magnetic field B is obtained by PFSS extrapolation from the magnetogram taken by Global Oscillation Network Group (GONG, Harvey 2011), and only the transverse component is used in the calculation.

2.4. Trigger mechanism

The trigger mechanisms of filament eruption, which have been introduced in Section 1, are classified into two types: reconnection and ideal MHD processes. Combining the soft X-ray flux, the time-distance map and the observations at onset time, we can distinguish which mechanism works in a filament eruption: for the reconnection-triggered events, the increase of soft X-ray flux, which corresponds to beginning of the associated flare, should be observed just ahead of the eruption onset time, and newly-formed flare ribbons or enhancements of emission intensity should be observed at the footpoints or spine of the erupting filament. In our events,

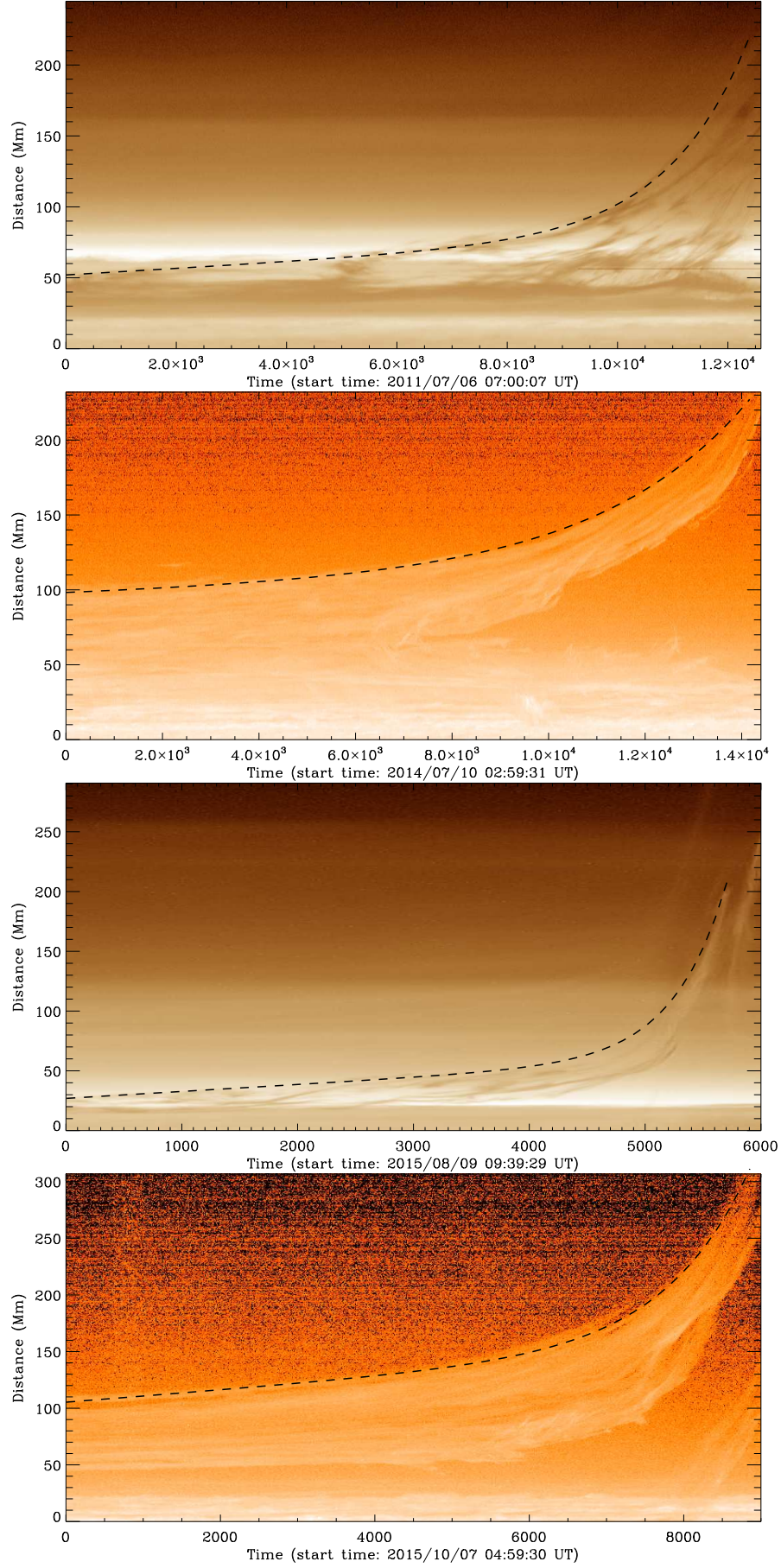


Figure 4. Four well-fit examples fitted with equation 1.

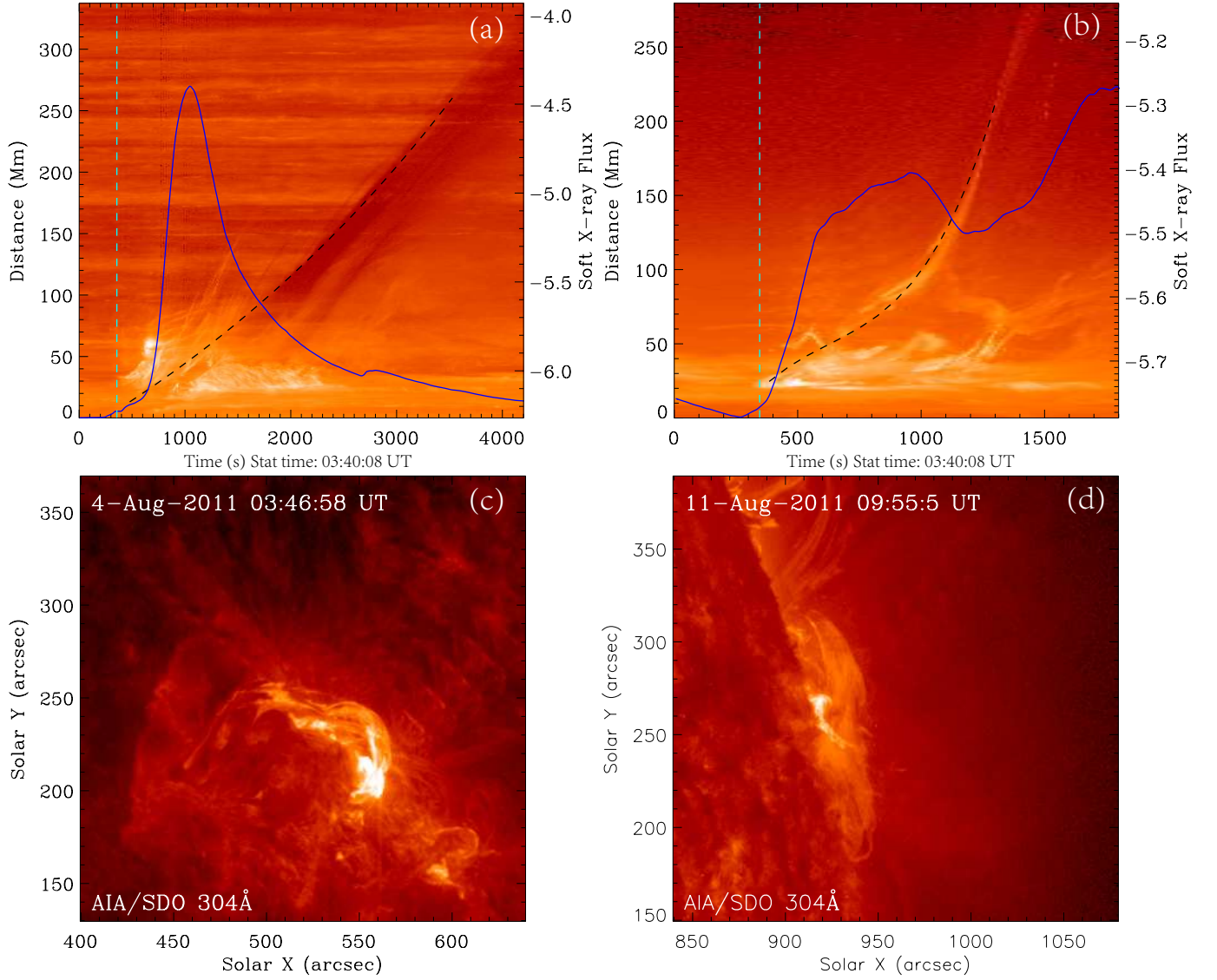


Figure 5. Samples for clarifying the reconnection triggered events. The black dashed lines in panels (a) and (b) are time-distance fitting curves, the blue lines are GOES soft X-ray flux, and cyan dashed lines indicate the onset time. Panels (c) and (d) are shown for the filaments observed at the onset time respectively.

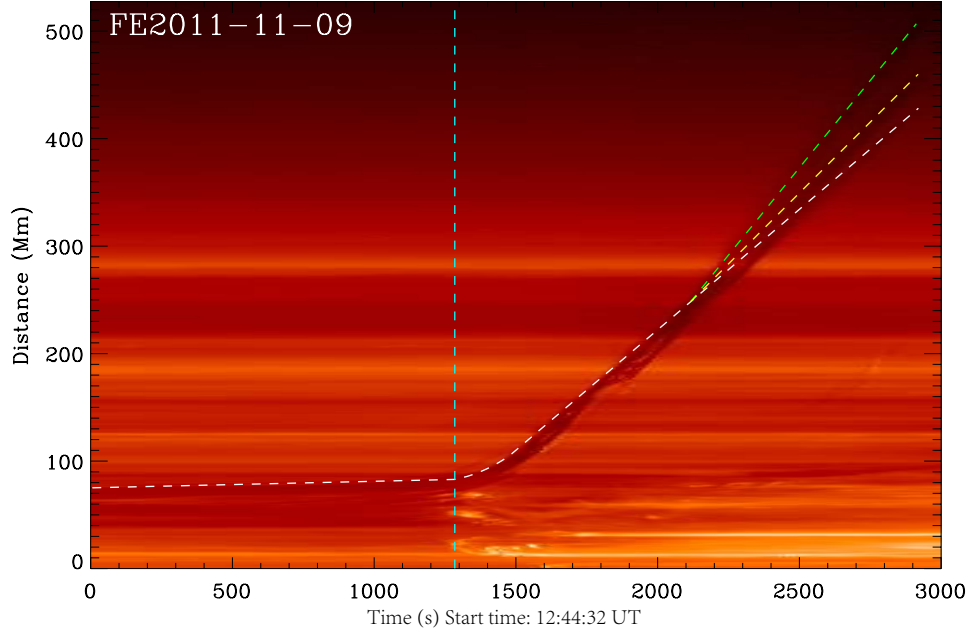


Figure 6. A sample of time-distance map that cannot be fitted by Equation 1. The white, yellow and green dashed lines are time-distance fitting curve. The cyan dashed line shows the onset time of this eruption.

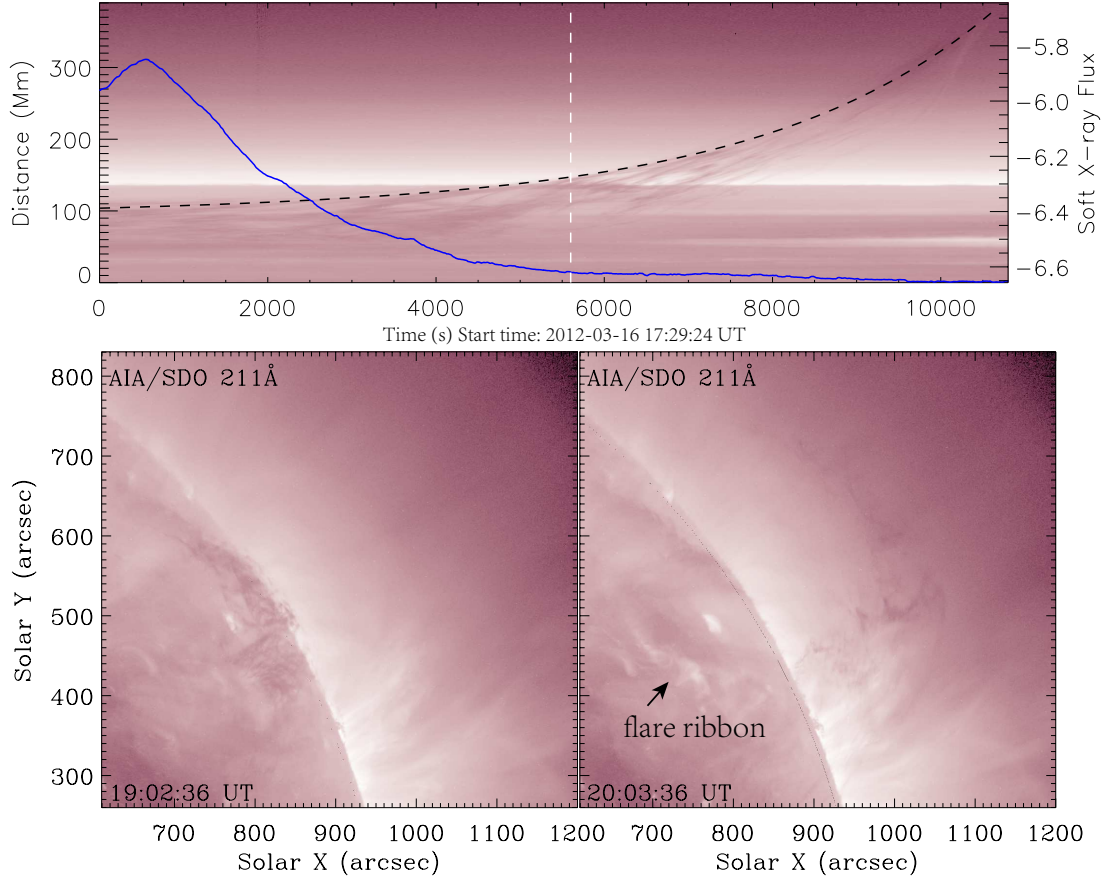


Figure 7. An example of non-reconnection triggered events. The top panel shows the time-distance map. The blue line is GOES soft X-ray flux, black dashed line is time-distance fitting curve and white dashed line shows the onset time. The bottom left panel shows the filament position at onset time and the bottom right panel shows the ribbons when it can clear be seen.

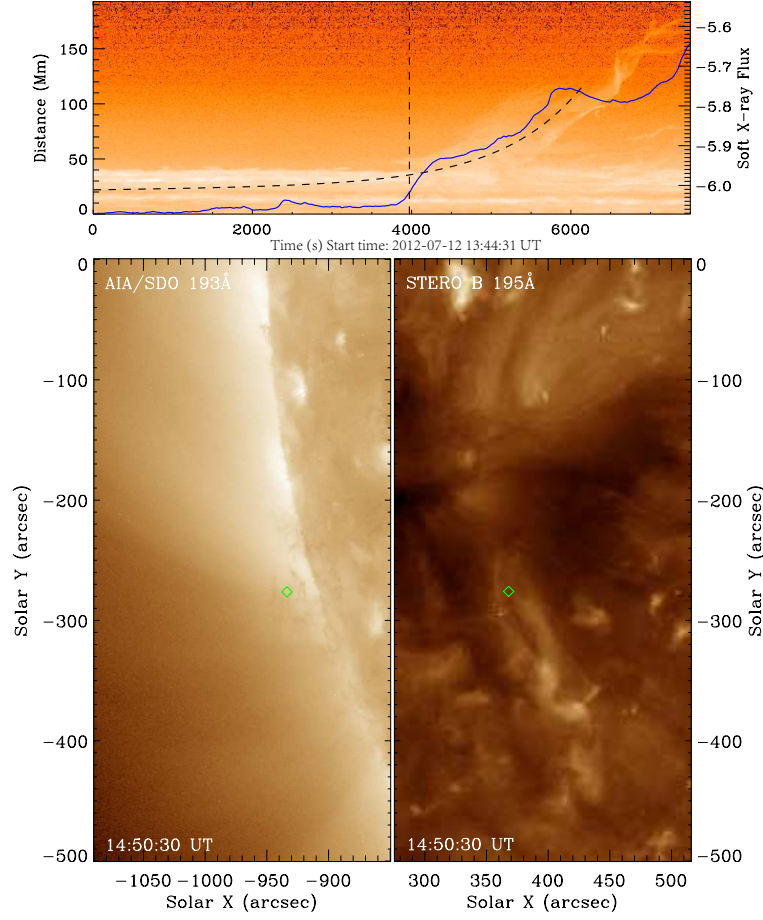


Figure 8. Example of non-reconnection triggered events. The top panel shows the time-distance map of non-reconnection triggered sample. The blue line is GOES soft X-ray flux, black dashed curve is time-distance fitting curve and the vertical black dashed line denotes the onset time. The bottom left panel shows the filament position at the onset time in AIA and panel c shows it in STEREO. The green diamond shows the same position of filament observed in the two facilities.

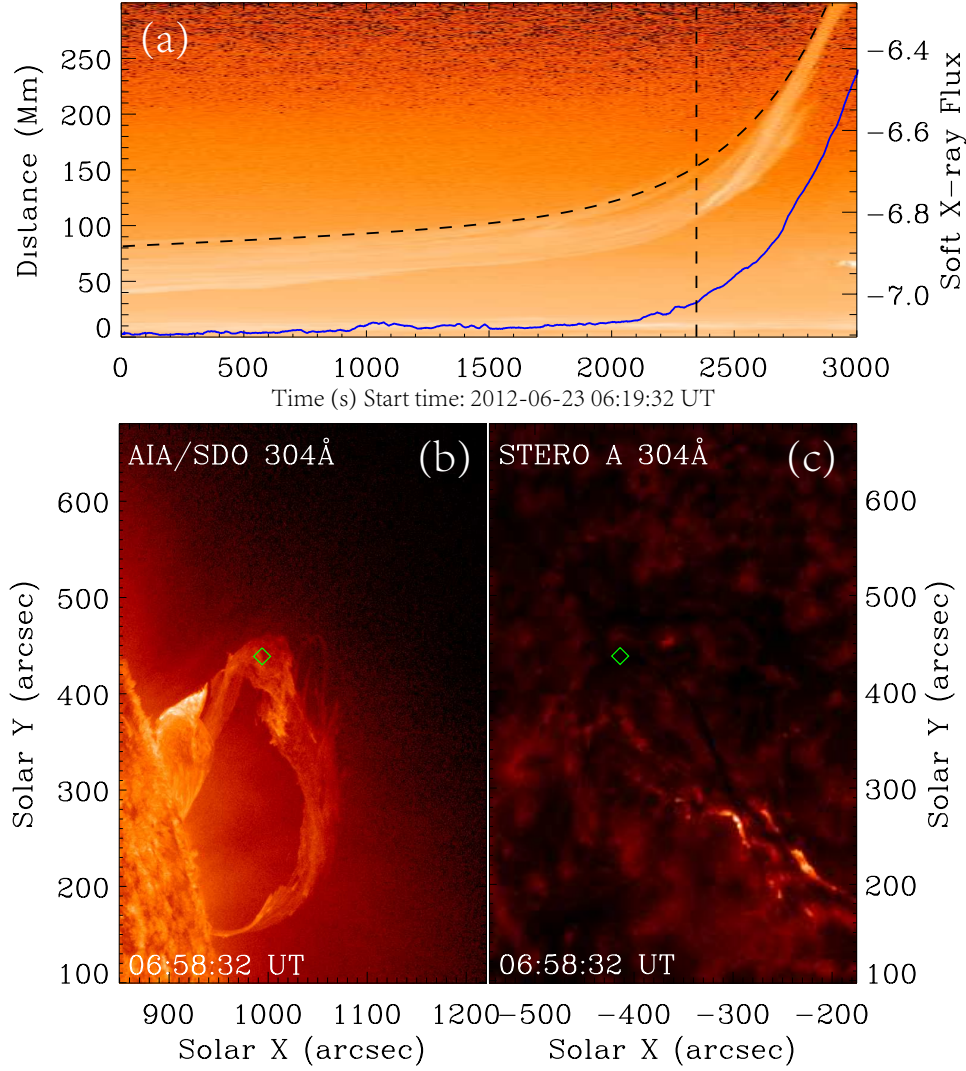


Figure 9. Same as Figure 8 but for a reconnection-triggered event.

some of them can unambiguously identified as being triggered by reconnection because the flare emission enhancements occur clearly before the onset of the fast rise eruption, for instance, see the sample shown in Figure 6. Two more samples of reconnection-triggered events are shown in Figure 5. Along with their time-distance maps, the observations at onset time are also exhibited. It can be seen that at onset time, both of their X-ray flux increased and the intensity enhancements can be seen in footpoint (panel c) and spine (panel d) of filament. On the contrary, a typical sample of eruptions triggered by non-reconnection processes are shown in Figure 7. It shows that there is no significant X-ray flux increasing before and at onset time and no significant radiative enhancements along the filament. Indeed, the associated flare ribbons appear almost one hour after the onset time of the filament eruption (see the last panel).

There are also some events which are difficult to determine the trigger mechanism using the above method, and we give

cautions for such cases. For example, in Figure 8, we present a QS prominence eruption event which appears to be triggered by reconnection but is actually not. The time-distance map shows that the GOES soft X-ray flux increased slightly before the eruption onset time (which is denoted by the vertical dashed line in panel a). However, by checking the 195 Å images taken by STEREO B, we find no flare ribbons or even no intensity enhancements associated with this eruption. We thus further examined the causes of the X-ray flux increasing and found that it was actually caused by an X1.4 flare occurs at an AR, NOAA 11520. Thus this event should be considered as triggered by ideal MHD process. For comparison, we also show a sample which have a similar situation, i.e., there is a small GOES emission increasing before the onset time of eruption (see Figure 9). At this time, there are no flares occurred in other active regions. Furthermore, from the observation of STEREO A, we find that underneath the erupting filament, there can obviously be seen the newly formed flare

ribbons, suggestion that this flare is accompanied with the filament eruption. Thus this eruption can be considered as being caused by reconnection.

However, some studies suggest that although the reconnection is observed prior to the onset time, it is still hard to say which mechanism is the trigger as the signatures of reconnection often coincides very closely to the onset of fast rising phase. Furthermore, even the reconnection begins well before the eruption, there is doubt that such reconnection is not a trigger, but an approach gradually building up the MFR to the state of loss of equilibrium or MHD instability (Vrsnak 1990, 2008; Aulanier et al. 2010). Thus we checked our reconnection-triggered events with more evidences by studying the decay index as well as the magnetic topology of their source regions. Firstly, the events for which the onset heights are far below the torus instability threshold are not likely triggered by torus instability. For the other events whose decay indexes are close to or even above the torus instability threshold (as listed in Table 1), the uncertainty on the trigger mechanism might be large since torus instability is also an option. However, as shown by their time-distance maps (e.g., Figure 6), we find the filaments are almost static without any rising motion before the reconnection occurs, and then they are strongly accelerated immediately after the reconnection onset. This means the reconnection is the key factor in breaking the equilibriums. Thus in such cases, it is more reasonable to consider that the eruptions are triggered by reconnection rather than torus instability. Furthermore, we checked the magnetic environments of the source region of these eruptions by analysing the photospheric magnetic flux distribution. It is believed that reconnection-triggered event is more likely to occur in complex magnetic topology than in the simple bipole field. For example, Moore & Sterling (2006) present three scenarios for reconnection-triggered eruptions under quadrupolar configuration. Consistently, we find that in our studied events, more than two thirds of the reconnection-triggered ones occurred in complex magnetic environments, e.g., a multipolar magnetic configuration. While for the non-reconnection triggered ones, more than two thirds occurred in simpler environment such as bipole field or the edge of ARs. Finally, it should be noted that there are events in which both reconnection and torus instability contribute to produce the eruption, as the reconnection first plays a role of trigger and shortly afterwards the torus instability sets in and further accelerates the filament.

3. RESULTS AND DISCUSSION

Here we summarize the results found basing on the data and analysis methods described in Section 2:

First, as shown in Figure 2, our statistic events includes 24 AR filaments, 11 IFs and 31 QS filaments but no PC filaments. In the statistical analysis of McCauley et al. (2015),

they mentioned that there are 19.6% AR filaments, 14.1% IFs, 51.3% QS filaments and 15% PC filaments. The difference in type ratios of our events with theirs suggests that high-speed CMEs result from AR filaments and IFs more frequently than QS and PC filaments. This is rather natural since the fast CMEs need more free magnetic energy (and stronger magnetic field) for large acceleration. It is worthy noting that there are still near 50% fast CMEs formed by eruptive QS filaments, which is more than that results from AR filaments. This indicates that the conversion ratio of free magnetic energy to CME's kinetic energy also plays an important role in determining CME acceleration. Such a conversion rate is probably related to magnetic environment of the eruptive filament. However, to determine this factor, one needs more comparative studies between eruptive AR filaments and QS filaments.

Second, as shown again in Figure 2, the eruptions triggered by reconnection are 62.5% for AR filaments, 36.4% for IFs and 16.1% for QS filaments. It shows that AR filament eruptions are preferred to be triggered by reconnection. The IF eruptions have a similar ratio between the reconnection and ideal-MHD triggers. On the other hand, the majority of the QS filament eruptions are triggered by ideal MHD mechanism, with only 5 events triggered by reconnection. It is commonly believed that due to the weak magnetic field, reconnection in QS area can hardly trigger a typical QS filament eruption with a large amount of mass. Thus we carefully check the movie of these 5 events to see why they are triggered by reconnection. We find that four of them (FE2012-05-11, FE2014-04-18, FE2015-04-04 and FE2015-08-23) are located at or close to the small poles which are not recognized as an active region, and the filaments are small as typical AR ones. It means they have a similar magnetic environment with relatively small AR filaments, thus the reconnection process are reasonable. Furthermore, the remaining one of the 5 events is triggered by an X-class flare in an AR which shows a very strange flare ribbons (FE2014-12-20). Its ribbons extend out of the AR and trigger the reconnection far away from the AR, then lead to the eruption of the QS filament. This is probably due to the complex magnetic environment there.

Third, the velocities of CMEs behave very differently between different filament types. As shown in Table 3, the average velocity of AR-filament formed CMEs is $1285.00 \text{ km s}^{-1}$, which is about 1.14 times of IF eruptions and 1.39 times of QS filament eruptions. This result for the fast CMEs differs significantly from the one summarized for all eruptions by McCauley et al. (2015). Unlike their results, the fast CMEs are prefer to be formed by AR filaments but not IFs. It means that magnetic strength plays an important role in acceleration of CME for the formation of fast CMEs, which is in agreement with the studies of some authors (Qiu &

Table 3. The CME velocities of different sets. (Unit: km s^{-1})

Type*	Average velocity	SE*	Max. velocity	Min. velocity
AR	1285.00	83.10	2508	812
AR/R	1293.60	93.71	2147	812
AR/NR	1270.67(1116.00)**	175.21(65.77)	2508(1471)	828
IF	1124.36	115.78	2175	810
IF/R	1270.50(969.00)	302.35(32.04)	2175(1014)	907
IF/NR	1040.86	76.11	1442	810
QS	921.00	23.15	1409	801
QS/R	843.60	21.15	926	805
QS/NR	932.04	26.83	1409	801
R	1196.00	82.27	2175	805
NR	1022.74	44.73	2508	801
M	1300.58	105.19	2175	812
C	1057.65	57.13	1867	805
UC	955.18	26.59	1409	801

* AR: AR filament, IF: Intermediate filament, QS: QS filament, R: reconnection, NR: non-reconnection, M: M-class flare, C: C-class flare, UC: under C-class flare and SE: standard error.

** bracket: the statistical results ignored the abnormal event.

Yurchyshyn 2005; Chen 2006). On the other hand, the trigger mechanisms, which are supposed to determine the initial acceleration of CMEs, i.e., the reconnection-triggered events always experience a impulsive and short acceleration phase and then evolve with a stable velocity, while the non-reconnection ones often show an exponential rising profile as described by Equation 1, play a less important role in determining the final velocity of CMEs. As can be seen, for whole data set, the average velocity of reconnection-triggered events is $1196.00 \text{ km s}^{-1}$ and for non-reconnection events is $1022.74 \text{ km s}^{-1}$, respectively. Interestingly, the average CMEs velocity of reconnection-triggered QS filament eruptions (843.60 km s^{-1}), is obviously smaller than those triggered by non-reconnection processes (932.04 km s^{-1}). This indicates that in weaker magnetic environment, the efficiency of acceleration via ideal MHD instability is higher than that via reconnection. For QS filaments and IFs, it seems the average velocities also have a big difference between reconnection triggered and non-reconnection triggered. But we find that there is one sample that diverges obviously from other samples in both two sets (FE2012-01-23 and FE2012-01-27), thus we also show the average velocities excluding these events in Table 3 with brackets. After excluding these two events, the difference is significantly reduced.

In previous works, the class of associated flares are also considered to be an important factor in accelerating the CME velocity (Hundhausen 1997; Yashiro et al. 2002; Vrsnak et al. 2005). Here we also analyse the relationship between CME velocities and associated flares. There are only 2 X-class flares and they are associated with the CMEs with highest velocities of above 2000 km s^{-1} . There are 12 M-class flares

events, and 10 are associated with AR filaments eruptions and 2 with IFs. There are 20 events associated with C-class flares, 9 of them are AR filament eruption, 5 of them are IFs and 6 of them are QS events. 27 events of the rest are associated with B-class flares or even weaker flare signal, 2 events have no record of GOES flux and 3 events covered by other flares. The average velocity of CMEs associated is $1300.58 \text{ km s}^{-1}$ for M-class flares, $1046.42 \text{ km s}^{-1}$ for C-class, and 956.08 km s^{-1} for B-class and below. Previously, Vrsnak et al. (2005) noticed that the CMEs associated with larger flares are generally faster and broader than those with small flares. Similar result is also found by Bein et al. (2012). Here we provide a more detailed evidence.

Last, the onset height and decay index are shown in Table 4. In order to clarify the effects of trigger mechanisms, we also divide them in two sets, i.e., reconnection and non-reconnection. Since there are only 2 events of reconnection-triggered QS filaments for which the onset height can be evaluated, thus they are ignored. It is found that the onset heights of AR filaments are close to the results of McCauley et al. (2015), but for the IFs and QS filaments, they are a bit higher. Interestingly, the decay indexes for different types behaves oppositely from McCauley et al. (2015)'s results, i.e., here the values for the AR filaments and IFs are higher while for the QS filaments they are close to McCauley et al. (2015)'s results. The higher decay index and the same onset height for AR filaments seems to imply that torus instability play a more important role in accelerating faster CMEs than in triggering the eruption. Furthermore, the average onset height (and also the decay index) of reconnection triggered AR filaments is a bit lower than that of non-reconnection triggered

Table 4. The onset height and decay index.

Type*	Onset height (Mm)	SE* (Mm)	Max. h (Mm)	Min. h (Mm)	Decay index	SE	Max DI*	Min DI
AR	43.44	6.43	115.8	11.5	1.45	0.13	2.47	0.4
AR/R	32.66	8.09	115.8	11.5	1.26	0.17	2.07	0.4
AR/NR	57.82	6.43	94.1	19.6	1.74	0.13	2.47	1.05
IF	68.88	6.68	98.9	38.6	1.35	0.16	2.20	0.76
IF/R	64.40	13.30	82.9	38.6	1.25	0.14	1.46	0.99
IF/NR	71.12	8.29	98.9	49.8	1.40	0.23	2.20	0.76
QS	100.29	13.78	344.1	20.0	1.24	0.10	2.41	0.66

* AR: AR filament, IF: Intermediate filament, QS: QS filament, SE: standard errors and DI: decay index.

ones. However, the most significant difference from [McCauley et al. \(2015\)](#)'s results is that the minimum decay index of reconnection-triggered ones are obviously lower. Indeed, we find the minimum decay index of non-reconnection samples are higher than 1, but for reconnection ones, the minimum is 0.4. Interestingly, the eruption with such low decay index is associated with a rather strong flare, i.e., an X4.9 class flare. Also, there are 36% samples have a decay index smaller than 1. We think it may explain the results summarized by [Jing et al. \(2018\)](#), i.e., strong enough reconnection can help magnetic structures break out the constrain of background field. But these differences are not found in IFs. Anyway, one should bear in mind that both of the onset heights and decay indexes have big uncertainties from direct observations. For prominences, we can get the onset heights reliably but to calculate the decay index, we can only use the magnetogram observed days before or after the eruption when the source region is observed on the solar disk. Similarly, for filaments, although the magnetogram are more accurate, the onset heights are less certain. Thus from this result we cannot make any strong conclusion, and a more meticulous work with more samples is needed.

4. SUMMARY

In this paper, by joint observations of SDO, STEREO GONG and GOES, we surveyed the eruption trigger mechanism for filaments that produced fast CMEs with velocity above 800 km s^{-1} observed from 2011 to 2017. The results of our statistical analysis can be summarized as follows:

(1) AR filament and IF eruptions show a higher probability for producing fast CMEs than QS filaments, while there is no PC filament eruptions producing fast CMEs in our statistic. This imply that stronger magnetic field can generate a fast CME more easily.

(2) The trigger mechanism show a significant difference between AR and QS filaments, i.e., AR filament eruptions

prefer to be triggered by reconnection while QS filament eruptions prefer to be triggered by non-reconnection process.

(3) The trigger mechanisms do not result in a significant difference in the CME speeds, except for QS filament eruptions, in which non-reconnection process can more likely generate a faster CME.

(4) Our statistic shows a trend that stronger flares are more likely associated with faster CMEs. This result is well in agreement with the previous results.

(5) The onset heights and decay indexes show differences from previous statistical works. It shows that torus instability may contribute more in accelerating faster CMEs. We also note that strong enough reconnection can break out the constrain of background field. However, due to the uncertainty of computing the onset heights and decay indexes, further works are needed for reconfirm this conclusion.

In summary, we find that QS filament eruptions still have a big enough ratio in leading to a faster CME, and they can transport free magnetic energy into kinetic energy of CMEs with higher efficiency. Thus, it is necessary to pay more attention in studying activities located in QS area for space weather forecast. The trigger mechanisms play further important roles in eruptive events. They show different behaviors in QS and AR filaments. For predicting an AR filament eruption, more attentions should be paid on the reconnection precursors, since the reconnection can trigger a fast eruption regardless the twist number ([Jing et al. 2018](#)) or even overlying magnetic field. But for QS filaments, more attention on overlying constrained field should be paid, since few reconnection events can lead a faster CME.

This work is supported by the National Natural Science Foundation of China (NSFC 41822404, 41731067, 41574170, 41531073), the Fundamental Research Funds for the Central Universities (Grant No.HIT.BRETIV.201901). P.Z. also acknowledges the support by China Postdoctoral Science Foundation (2018M641812). Data from observations are courtesy of NASA SDO/AIA and the HMI science teams.

REFERENCES

- Antiochos, S. K., DeVore, C. R. & Klimchuk, J. A. 1999, *ApJ*, 510, 485
- Aulanier, G., Török, T., Demoulin, P. & DeLuca, E. E. 2010, *ApJ*, 708, 314
- Bein, B. M., Berkebile-Stoiser, S., Veronig, A. M., Temmer, M. & Vrsnak, B. 2012, *ApJ*, 755, 44
- Chen, A. Q., Chen, P. F. & Fang, C., 2006, *A&A*, 456, 1153
- Chen, P. F. & Shibata, K. 2000, *ApJ*, 545, 524
- Chen, P. F. 2011, *LRSP*, 8, 1
- Cheng, X., Zhang, J., Ding, M. D., Olmedo, O., Sun, X. D., Guo, Y. & Liu, Y. 2013, *ApJL*, 769, L25
- Engvold, O. 2015, Description and classification of prominences. In: Vial, J.-C., Engvold, O. (eds.) *Solar Prominences*, *Astrophys. Space Sci. Lib.*, 415, 31
- Feynman, J. & Martin, S.F. 1995, *J. Geophys. Res.*, 100, 3355
- Goff, C. P., van Driel-Gesztelyi, L., Harra, L. K., Matthews, S. A. & Mandrini, C. H. 2005, *A&A*, 434, 761
- Gonzalez, W. D., Tsurutani, B. T. & Clua de Gonzalez, A. L. 1992, *Space Sci. Rev.*, 88, 529
- Gopalswamy, N. & Kundu, M. R. 1992, *ApJL*, 390, 37
- Gopalswamy, N., Lara, A., Yashiro, S., Nunes, S. & Howard, R. A. 2003, in *Solar Variability as an Input to the Earth's Environment*, Eds. Wilson, A., SP-535, 403
- Harrison, R. A. 1995, *A&A*, 304, 585
- Harvey, J. W., Bolding, J., Clark, R., et al. 2011, *BAAS*, 42, 17.45
- Howard, R. A., Moses, J. D., Vourlidas, A., et al. 2008, *Space Sci. Rev.*, 136, 67
- Hudson, H. S., Acton, L. W. & Freeland, S. L. 1996, *ApJ*, 470, 629
- Hurlburt, N., Cheung, M., Schrijver, C., et al. 2012, *SoPh*, 275, 67
- Huttunen, K. E. J., Koskinen, H. E. J., Schwenn, R. & Dal Lago, A. 2002, in *Solar Variability: From Core to Outer Frontiers*, Eds. Wilson, A., SP-506, 137
- Huttunen, K. E. J., Schwenn, R., Bothmer, V. & Koskinen, H. E. J. 2005, *Ann. Geophys.*, 23, 625
- Hundhausen, A. J. 1997, in *Cosmic Winds and the Heliosphere*, (Eds.) Jokipii, J.R., Sonett, C.P., Giampapa, M.S., *Space Science Series*, pp. 259–296, Arizona University Press, Tucson
- Jackson, B. V. 1985, *Sol. Phys.*, 100, 563
- Jing, J., Yurchyshyn, V. B., Yang, G., Xu, Y. & Wang, H. 2004, *ApJ*, 614, 1054
- Jing, J., Liu, C., Lee, J., Ji, H., Liu, N., Xu, Y. & Wang, H. 2018, *ApJ*, 864, 138
- Kippenhahn, R., & Schluter, A. 1957, *ZA*, 43, 36
- Kliem, B. & Török, T. 2006, *Phys. Rev. Lett.*, 96, 255002
- Kuperus, M., & Raadu, M. A. 1974, *A&A*, 31, 189
- Leka, K. D., Canfield, R. C., McClymont, A. N., & van Driel-Gesztelyi, L. 1996, *ApJ*, 462, 547
- Lemen, J. R., Title, A. M., Akin, D. J., et al. 2012, *SoPh*, 275, 17
- Liu, Y., Zhao, J., Schuck, P. W., 2012, *Sol. Phys.*, 287, 279
- Liu, Y. D., Luhmann, J. G., Kajdic, P., et al. 2014, *Nat. Commun.*, 5, 3481
- Lynch, B. J., Antiochos, S. K., MacNeice, P. J., et al. 2004, *ApJ*, 617, 589
- McCauley, P. I., Su, Y. N., Schanche, N. et al. 2015, *SoPh*, 290, 1703
- Moore, R. L., Sterling, A. C., Hudson, H. S. & Lemen, J. R. 2001, *ApJ*, 552, 833
- Moore, R. L. & Sterling, A. C., 2006, Initiation of Coronal Mass Ejections, in *Washington DC American Geophysical Union Geophysical Monograph Series*, 165, 43
- Pesnell, W. D., Thompson, B. J. & Chamberlin, P. C. 2012, *Sol. Phys.*, 275, 3
- Qiu, J. & Yurchyshyn, V. B. 2005, *ApJL*, 634, L121
- Sakurai, T. 1976, *Publ. Astron. Soc. Japan*, 28, 177
- Singer, H. J., Heckman, G. R. & Hirman, J. W. 2001, in *Space Weather*, Ed. Song, P. et al., 125, 23
- Schwenn, R., dal Lago, A., Huttunen, E. & Gonzalez, W. D. 2005, *Ann. Geophys.*, 23, 1033
- Shimizu, T., Lites, B. W., & Bamba, Y. 2014, *PASJ*, 66, 14
- Sterling, A. C. & Moore, R. L. 2001, *ApJ*, 560, 1045
- Sterling, A. C. & Moore, R. L. 2001, *ApJ*, 561, 219
- Sterling, A. C. & Moore, R. L. 2005, *ApJ*, 630, 1148
- Sterling, A. C., Chifor, C., Mason, H. E., Moore, R. L., & Young, P. R. 2010, *A&A*, 521, A49
- Su, Y., van Ballegooijen, A., MacCauley, P., et al. 2015, *ApJ*, 807, 144
- Török, T. & Kliem, B. 2005, *ApJL*, 630, L97
- Tsurutani, B. T., Smith, E. J., Gonzalez, W. D., Tang, F. & Akasofu, S. I. 2014, *J. Geophys. Res.*, 93, 8519
- van Ballegooijen, A. A. & Martens, P. C. H. 1989, *ApJ*, 343, 971
- Vrsnak, B. 1990, *Sol. Phys.*, 129, 295
- Vrsnak, B. 2008, *Annales Geophysicae*, 26, 3089
- Vrsnak, B., Sudar, D. & Ruzdjak, D. 2005, *A&A*, 435, 1149
- Wang, H., Liu, C., Deng, Y., & Zhang, H. 2005, *ApJ*, 627, 1031
- Wang, Y. & Zhang, J. 2007, *ApJ*, 665, 1428
- Williams, D. R., Török, T., Demoulin, P., van Driel-Gesztelyi, L. & Kliem, B. 2005, *ApJL*, 628, L163
- Yashiro, S., Gopalswamy, N., Michalek, G. & Howard, R. A. 2002, *Bull. Am. Astron. Soc.*, 34, 695
- Yashiro, S., Gopalswamy, N., Akiyama, S., Michalek, G. & Howard, R. A. 2005, *J. Geophys. Res.*, 110, A12S05
- Yang, S., Zhang, J., Zhu, X. & Song, Q. 2017, *ApJ*, 849, 21
- Zhou, G. P., Wang, J. X., Zhang, J. et al. 2006, *ApJ*, 651, 1238
- Zhou, G. P., Zhang, J., Wang, J. X. & Wheatland, M. S. 2017, *ApJL*, 851, L1